

Growth of Velocity Dispersions for Collapsing Spherical Stellar Systems

Shunsuke HOZUMI

Faculty of Education, Shiga University, 2-5-1 Hiratsu, Otsu 520

E-mail: hozumi@sue.shiga-u.ac.jp

Takao FUJIWARA

Kyoto City University of Arts, Nishikyo-ku, Kyoto 610-11

and

Yukitoshi KAN-YA

Department of Physics, Faculty of Science, Kyoto University,

Sakyo-ku, Kyoto 606

(Received 1996 February 5; accepted)

Abstract

First, we have ensured that spherical nonrotating collisionless systems collapse with almost retaining spherical configurations during initial contraction phases even if they are allowed to collapse three-dimensionally. Next, on the assumption of spherical symmetry, we examine the evolution of velocity dispersions with collapse for the systems which have uniform or power-law density profiles with Maxwellian velocity distributions by integrating the collisionless Boltzmann equation directly. The results show that as far as the initial contraction phases are concerned, the radial velocity dispersion never grows faster than the tangential velocity dispersion except at small radii where the nearly isothermal nature remains, irrespective of the density profiles and virial ratios. This implies that velocity anisotropy as an initial condition should be a poor indicator for the radial orbit instability. The growing behavior of the velocity dispersions is briefly discussed from the viewpoint that phase space density is conserved in collisionless systems.

Key words: Galaxies: formation — Galaxies: structure — Instabilities — Methods: numerical — Stellar dynamics

1. Introduction

Since van Albada (1982) demonstrated that collapse of stellar systems with small initial virial ratios leads to the end products whose density pro-

files are well-described by the de Vaucouleurs $R^{1/4}$ law in projection, much attention has been paid to cold dissipationless collapse from the standpoint of the formation of elliptical galaxies. In addition, it has been found from collapse simulations (Polyachenko 1981, 1992; Merritt and Aguilar 1985; Barnes et al. 1986; Aguilar and Merritt 1990; Londrillo et al. 1991; Udry 1993) that cold enough systems are deformed into triaxial configurations by the radial orbit instability (ROI). On the other hand, observations suggest that elliptical galaxies are triaxial systems supported by anisotropic velocity dispersions (Franx et al. 1991). Putting these things together, we may favor the view that the ROI accompanied by cold collapse can naturally explain the observed properties of elliptical galaxies.

In spite of the importance of the ROI, its physical mechanism remains still uncertain. Many workers have searched for the criterion of the ROI from the initial conditions adopted. In particular, velocity anisotropy is considered a key ingredient because the ROI could be a kind of Jeans instability in the tangential direction as stated by Merritt (1987). Although the ROI appears to occur in systems with larger velocity dispersion in the radial direction than in the tangential direction, Udry (1993) has reported that for centrally concentrated density profiles, triaxial systems formed through the ROI even in the initial anisotropic models characterized by $2T_{\text{rad}}/T_{\perp} \ll 1$, where T_{rad} and T_{\perp} are the kinetic energies in radial and tangential motions, respectively. In retrospect, velocity anisotropy as an initial condition may have nothing to do with the ROI. In fact, numerical studies carried out so far demonstrate that collapsing spherical nonrotating systems remain spherical until around the maximum collapse times at which the virial ratios become maximum (see e.g., Figure 3 of Aguilar and Merritt 1990). Nevertheless, no one has argued the velocity anisotropy just before the onset of the ROI.

These studies mentioned above indicate that we still lack the exact knowledge of how the velocity dispersions of stellar systems, initially far from equilibrium, evolve with collapse. Recently, Kan-ya et al. (1995) have shown that for spherically symmetric stellar systems the tangential velocity dispersion grows faster than the radial one as far as the initial contraction phases are concerned. Unfortunately, however, their analyses are based on such a cold approximation that the system has nearly zero velocity dispersions initially. In reality, stellar systems would form with some degree of velocity dispersion. If the system with a power-law density profile has velocity dispersion at its birth, individual mass shells can overlap with one another during the collapse,

which is then likely to affect the growing behavior of the velocity dispersions. Aside from the cold approximation, they analyzed the systems on the basis of spherical symmetry. Consequently, we cannot apply their results directly to real galaxies which would have collapsed three-dimensionally. Therefore, we need to unravel the collapsing behavior of stellar systems at early stages, and then investigate the growing behavior of the velocity dispersions which they have from the beginning.

First, in section 2, we ensure that spherical stellar systems evolve without deviating from spherical configurations at the early stages of gravitational collapse. Next, in section 3, on the assumption of spherical symmetry, we study the growing behavior of velocity dispersions for the systems which have uniform or power-law density profiles. Discussion and conclusions are presented in section 4.

2. Collapsing Behavior of Spherical Systems

We first study how spherical stellar systems, initially far from equilibrium, collapse three-dimensionally at the early stages of contraction. Above all, the time evolution of axis ratios, b/a and c/a , is presented, where a , b , and c are the major, intermediate, and minor axes, respectively.

We use the self-consistent field (SCF) method, termed by Hernquist and Ostriker (1992), to study the collapsing behavior of spherical stellar systems. Since the SCF method requires no introduction of a softening length, it is suitable to cold collapse simulations in which the modification of a central force field through a softening length can have a large effect on the global dynamics. In addition, the reliability of the SCF method is demonstrated by Hozumi and Hernquist (1995) who applied it to spherically symmetric systems. In the present simulations, we no longer restrict ourselves to spherical symmetry. Thus, the angular dependence of the density and potential as well as the radial one is expanded in the SCF code. Since collapse simulations reveal that density profiles of the end products resemble galaxies obeying the de Vaucouleurs $R^{1/4}$ law in projection, we choose the basis set proposed by Hernquist and Ostriker (1992) on the ground that its lowest order members accurately describe spheroidal objects like elliptical galaxies (Hernquist 1990). We adopt $n_{\max} = 16$ and $l_{\max} = m_{\max} = 6$, where n_{\max} is the maximum number of radial expansion coefficients and l_{\max} and

m_{\max} are the maximum numbers of angular expansion coefficients. We employ $N = 100,000$ particles of equal mass. The equations of motion are integrated in Cartesian coordinates using a time-centered leapfrog algorithm (e.g., Press et al. 1986).

The initial conditions consist of those spherical systems of total mass M and radius R_0 which have density profiles of $\rho(r) \propto r^{-n}$, where n is chosen to be 0 and 1. The velocity distributions are Maxwellian with the dispersions determined from the virial ratio, $|2T/W|=10^{-1.5}$, where T and W denote the kinetic and gravitational energies, respectively, although the velocities are assigned so that the initial data do not include escapers. The unit of mass and the gravitational constant, G , are taken so that $M = 1$ and $G = 1$. The unit of length is determined from the relation such that $|2T/W| \times R_0 = 1$. Then, we choose the length scale of the basis functions to be 2.

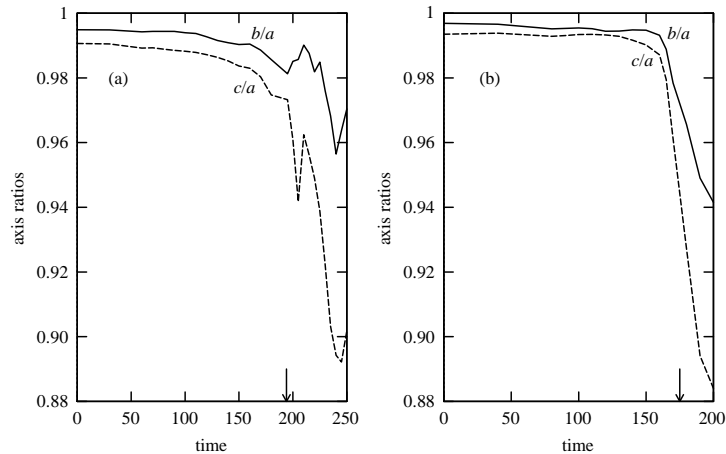


Fig. 1. Evolution of the axis ratios for (a) the uniform density sphere and (b) the $\rho \propto r^{-1}$ model. The virial ratios are chosen to be $10^{-1.5}$. The solid lines show b/a and the dashed lines c/a , where a , b , and c denote the major, intermediate, and minor axes, respectively. The vertical arrows indicate the maximum collapse times.

In figures 1a and 1b, we present the time evolution of the axis ratios, b/a and c/a for $n = 0$ and 1, respectively. The axis ratios are computed from the principal moments of inertia for the most bound 80% of the particles. We stop the simulations just after the maximum collapse times because we pay attention only to the early stages of gravitational collapse. According to Cannizzo

and Hollister (1992), the final elongation becomes larger as the initial density profile is more centrally concentrated provided that the initial virial ratio is fixed. However, as far as the initial contraction phases are concerned, we can see that the systems approach the maximum collapse times with almost retaining spherical configurations, irrespective of the initial density profiles. In fact, figure 1b shows that the axis ratios change little from the initial values of $b/a = 0.997$ and $c/a = 0.993$ during the early contraction times (from $t = 0$ to $t \approx 170$) even for the $n = 1$ density profile model. The small deviations of b/a and c/a from unity before the maximum collapse phases are, in large measure, considered root-mean-square fluctuations coming from finite numbers of particles used in the simulations. We conclude, therefore, that spherical stellar systems which have uniform or power-law density profiles do not deviate considerably from spherical configurations during the early stages of contraction even if they are allowed to collapse three-dimensionally.

3. Growing Behavior of Velocity Dispersions

We have demonstrated in section 2 that spherical stellar systems collapse symmetrically in configuration to a considerable degree at the early stages of contraction. Thus, spherical symmetry can be a good assumption when we study the growing behavior of velocity dispersions for such systems as long as their evolution stays in the initial contraction phases.

3.1. Analytical Predictions

Before proceeding into numerical simulations, we summarize the growing behavior of the velocity dispersions predicted from analytical results. In figure 2, we reproduce the evolution of the velocity dispersions for spherical symmetric systems on the basis of Kan-ya et al.'s (1995) analyses. It can be noticed from figure 2a that for the uniform density sphere the radial velocity dispersion grows exactly in the same manner as the tangential one and that the growth of both the dispersions is independent of radius. Figures 2b and 2c show that for the power-law density spheres the radial velocity dispersions decrease after some collapse time, while the tangential velocity dispersions continue to increase with time at all radii. In particular, the radial velocity dispersions decrease inward radially after some collapse time for the $\rho \propto r^{-0.5}$

model, and always decrease inward radially for the $\rho \propto r^{-1}$ model. Of course, this behavior of the radial velocity dispersion comes from Kan-ya et al.'s (1995) assumption that the system can continue to contract infinitely. Furthermore, they neglect the existence of the outer edges. Therefore, their analyses would apply to some intermediate radii of the systems which have finite extent and some degree of velocity dispersion from the beginning.

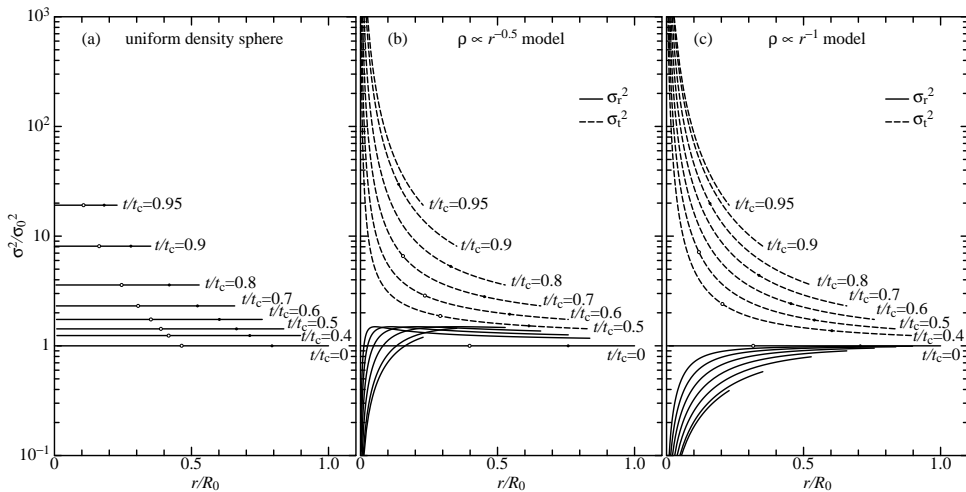


Fig. 2. Evolution of the velocity dispersions on the assumption that the effects of velocity dispersions are small enough, for (a) the uniform density sphere, (b) the $\rho \propto r^{-0.5}$ model, and (c) the $\rho \propto r^{-1}$ model. The solid lines show the square of the radial velocity dispersion σ_r^2 , and the dashed lines that of the tangential velocity dispersion σ_t^2 . Note that the evolution of the radial velocity dispersion is exactly the same as that of the tangential velocity dispersion for the uniform density sphere. The velocity dispersions and the radius are normalized with the initial value σ_0^2 and the cutoff radius R_0 , respectively. The circles are added on the σ_t^2 lines to indicate the evolutionary stages of the collapse: the filled circle is the half mass radius and the open circle the radius within which the system contains 10 % of the total mass. The time t_c is the collapse time at the cutoff radius R_0 .

In summary, we can see that the growing rate of the radial velocity dispersion never exceeds that of the tangential one with a cold approximation. In particular, for the power-law density spheres, the ratio of the radial to

tangential velocity dispersions becomes smaller as time proceeds. In addition, the decrease of the ratio is accelerated as the density gradient becomes steeper.

3.2. Numerical Results

Now that spherical symmetry is adopted, we use a phase-space method developed by Fujiwara (1983) because it gives desirable results insusceptible to random fluctuations. This method enables us to obtain a smooth distribution of velocity dispersions along radius. We employ $(N_r, N_u, N_j) = (150, 151, 80)$, where N_r , N_u , and N_j are the numbers of mesh points along radius, radial velocity, and angular momentum, respectively. The units of mass, M , and the gravitational constant, G , are taken so that $M = 1$ and $G = 1$. The unit of length is determined from the relation such that $|2T/W| \times R_0 = 1$ as in section 2.

We examine the time evolution of the velocity dispersions by gravitational collapse for density profiles of $\rho(r) \propto r^{-n}$ with Maxwellian velocity distributions, where $n=0$, $1/2$, and 1 are chosen, on the assumption of spherical symmetry. The initial virial ratios are taken to be $10^{-1.5}$, 10^{-1} , and $10^{-0.5}$ for each value of n .

In figure 3, the time evolution of σ_r^2 and σ_t^2 is shown for the uniform density spheres, i.e., $n=0$, where σ_r and σ_t are the radial and tangential velocity dispersions, respectively. It can be noticed that the evolution of σ_r^2 and σ_t^2 is very similar to one another, regardless of the initial virial ratios. That is, both the velocity dispersions grow at the same rate within some radius, which means that the systems keep the isothermal nature there as indicated by the analytical predictions. The outer regions, however, show the deviation from them. This is because the velocity dispersions which the system has from the beginning operate to blur the outer edge: the spread of the radial velocity becomes smaller outward to the edge. In this way, the isothermal nature disappears with time from outside. This effect is more prominent for the larger initial virial ratios. Therefore, the coldest model shows the abrupt drop in the radial velocity dispersion (figure 3a), while the other models show the gentle decrease of it (figures 3b and 3c).

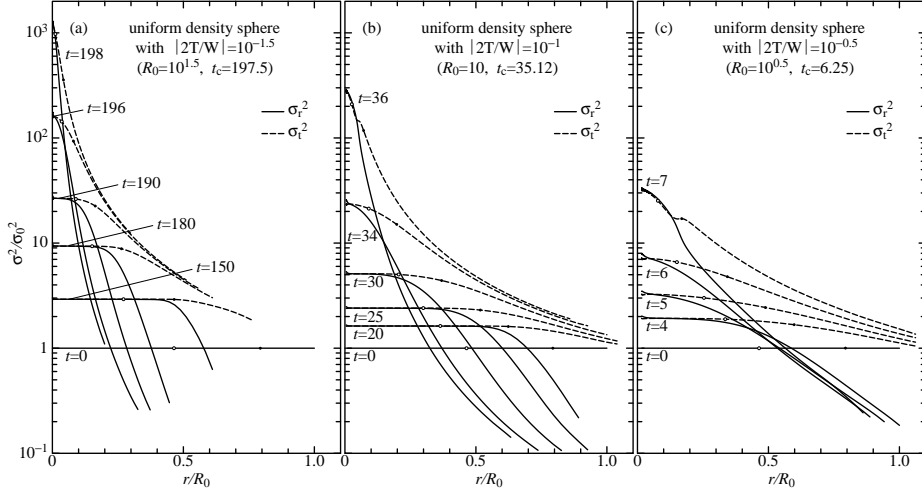


Fig. 3. Evolution of the velocity dispersions for the uniform density spheres with initial virial ratios (a) $|2T/W|=10^{-1.5}$, (b) $|2T/W|=10^{-1}$, and (c) $|2T/W|=10^{-0.5}$. The solid lines show the square of the radial velocity dispersion σ_r^2 and the dashed lines that of the tangential velocity dispersion σ_t^2 . The velocity dispersions and the radius are normalized with the initial value σ_0^2 and the cutoff radius R_0 , respectively. The filled circle is the half mass radius and the open circle the radius within which the system contains 10 % of the total mass. The time t_c is the collapse time at the cutoff radius R_0 with no initial velocity dispersion.

In figures 4 and 5, we present the time evolution of σ_r^2 and σ_t^2 for the $\rho \propto r^{-0.5}$ and $\rho \propto r^{-1}$ models, respectively. Now, let us focus on figures 4a and 5a. If we pay attention to the intermediate radii, the tendency of the evolution of both the velocity dispersions agrees roughly with that predicted by the analytical results (see figures 2b and 2c). In the central region, however, the nearly isothermal evolution can be seen, which differs from the analytical results. This is because the velocity dispersions prevent the system from contracting infinitely. In fact, the density near the central region was kept approximately uniform throughout the contracting phase. Thus, the evolution of the central part resembles that of the uniform density spheres: both the radial and tangential velocity dispersions increase in the same manner as the system collapses. The deviation from the analytical predictions also appears near the outer edges. The same reason as described for the uniform

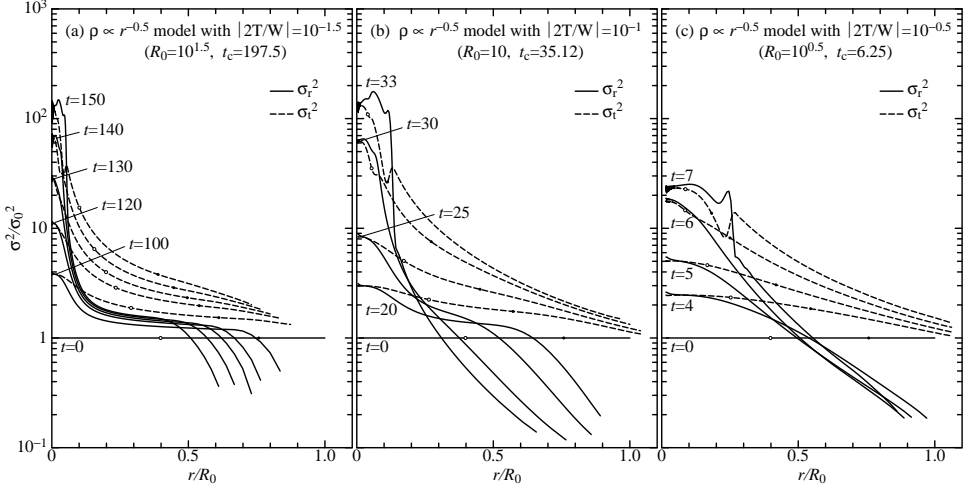


Fig. 4. Evolution of the velocity dispersions for the $\rho \propto r^{-0.5}$ models with initial virial ratios (a) $|2T/W|=10^{-1.5}$, (b) $|2T/W|=10^{-1}$, and (c) $|2T/W|=10^{-0.5}$. The notations and their meanings are the same as in figure 2.

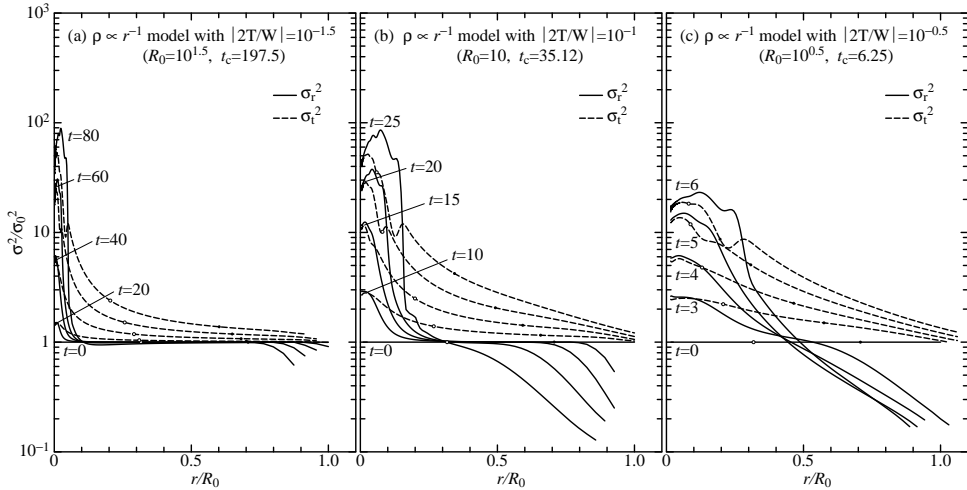


Fig. 5. Evolution of the velocity dispersions for the $\rho \propto r^{-1}$ models with initial virial ratios (a) $|2T/W|=10^{-1.5}$, (b) $|2T/W|=10^{-1}$, and (c) $|2T/W|=10^{-0.5}$. The notations and their meanings are the same as in figure 2.

density spheres can be applied to the decrease of the radial velocity dispersion near the edges. The larger amount of velocity dispersion does not change largely the evolution of σ_r^2 and σ_t^2 as can be seen from figures 4b, 4c, 5b, and 5c.

4. Discussion and Conclusions

We have found that spherical nonrotating systems keep their spherical configurations during the collapse at the early stages of contraction. We thus carried out collapse simulations on the assumption of spherical symmetry to examine how the velocity dispersions of spherical stellar systems evolve with collapse. Then, we have demonstrated that the radial velocity dispersion never grows faster than the tangential velocity dispersion except at small radii where the nearly isothermal nature is retained up to around the maximum collapse times, irrespective of the initial density profiles and virial ratios.

Our results are basically consistent with those of Kan-ya et al. (1995), although they assume that initial systems have nearly zero velocity dispersions. Thus, we can see that in general the system just before the onset of the ROI has larger velocity dispersion in the tangential direction than in the radial direction, which might be different from the situation that we envisage for the occurrence of the ROI. However, these findings can be understood qualitatively with relative ease as follows. If the initial density distribution is uniform, the collapse time of the system is independent of radius, so that the conservation of phase space density results in $\sigma_R \times R = \text{const.}$, where σ_R and R denote the characteristic radial velocity dispersion and radius of the system, respectively. In addition, the conservation of angular momentum of each star leads to $\sigma_T \times R = \text{const.}$, where σ_T is the characteristic one-dimensional tangential velocity dispersion. Then, the ratio, σ_R/σ_T , remains unity during the early stages of contraction when the system starts with an isotropic velocity distribution. On the other hand, if the initial density distribution is power-law such as $\rho \propto r^{-n}$ ($n > 0$), the stars of inner parts fall first and then those of outer parts follow. Consequently, the width of the radial velocity spread for the power-law density profiles is narrower than that for the uniform density profiles while $\sigma_T \times R = \text{const.}$ still holds. It may be helpful to remind that the collapse time of the outer edge for the power-law density spheres is the same as that for the uniform density spheres.

As a result, the ratio, σ_R/σ_T , continues to decrease from its initial value of unity with time if the system has a power-law density profile and an isotropic velocity distribution at the beginning.

In the numerical simulations, the deviation of the evolution of the velocity dispersions from the analytical results emerges at small radii for the power-law density profiles and near the edge of the system for the uniform and power-law density profiles. Since the system has finite extent, the velocity difference of the phase space elements makes the radial velocity dispersion smaller near the edge as collapse proceeds. On the other hand, the velocity dispersions can save the system from contracting infinitely. Then, the conservation of phase space density again means the increase of the radial velocity dispersion as the system contracts. Concerning the isothermal nature at small radii, we point out that the density near the central region was kept approximately uniform with collapse.

We can now explain why the collapse simulations thus far have shown that spherical systems approached the maximum collapse phases with retaining their initial shapes. This is because the tangential velocity dispersion remains equal to or overwhelms the radial one as collapse proceeds. Conversely, the predominance of the growth of the tangential velocity dispersion prevents the system from being deformed into elongated configurations at early collapse phases. It is thus suggested that the onset of the ROI is determined from the physical conditions at least just before or around the maximum collapse phase. Even though we start with the condition that $2T_{\text{rad}}/T_{\perp} > 1$, the growth of the tangential velocity dispersion can easily catch up with or exceed that of the radial velocity dispersion if the system has a power-law density distribution. Since we have found that the criterion of the ROI will not depend strongly on the initial velocity anisotropy, it is no wonder that small values such that $2T_{\text{rad}}/T_{\perp} \ll 1$ lead to triaxial end products as reported by Udry (1993). Therefore, we conclude that initial anisotropy parameters like $2T_{\text{rad}}/T_{\perp}$ should be a poor indicator for the ROI.

We are grateful to Professors S. Kato and S. Inagaki for their careful reading of the manuscript and helpful comments on its contents.

References

Aguilar L.A., Merritt D.R. 1990, ApJ 265, 33

- Barnes J.E., Goodman J., Hut P. 1986, *ApJ* 300, 122
 Cannizzo J.K., Hollister T.C. 1992, *ApJ* 400, 58
 Franx M., Illingworth G.D., de Zeeuw P.T. 1991, *ApJ* 383, 112
 Fujiwara T. 1983, *PASJ* 35, 547
 Hernquist L. 1990, *ApJ* 356, 359
 Hernquist L., Ostriker J.P. 1992, *ApJ* 386, 375
 Hozumi S., Hernquist L. 1995, *ApJ* 440, 60
 Kan-ya Y., Sasaki M., Tsuchiya T., Gouda N. 1995, Submitted to *Prog. Theor. Phys.*
 Londrillo P., Messina A., Stiavelli M. 1991, *MNRAS* 250, 54
 Merritt D.R. 1987, in *Structure and Dynamics of Elliptical Galaxies*, IAU Symp. No. 127, ed. P.T. de Zeeuw (Reidel, Dordrecht), p315
 Merritt D.R., Aguilar L.A. 1985, *MNRAS* 217, 787
 Polyachenko V.L. 1981, *SvA* L7, 79
 Polyachenko V.L. 1992, *SvA* 36, 482
 Press W.H., Flannery B.P., Teukolsky S.A., Vetterling W.T. 1986, in *Numerical Recipes: The Art of Scientific Computing* (Cambridge University Press, Cambridge)
 Udry, S. 1993, *A&A* 268, 35
 van Albada T.S. 1982, *MNRAS* 201, 939